UNIVERSITY OF CALIFORNIA

Los Angeles

Towards Quantum State Resolved Ion-Molecule Chemistry

A dissertation submitted in partial satisfaction

of the requirements for the degree

Doctor of Philosophy in Physics

by

Gary Chen

2019

© Copyright by
Gary Chen
2019

ABSTRACT OF THE DISSERTATION

Towards Quantum State Resolved Ion-Molecule Chemistry

by

Gary Chen
Doctor of Philosophy in Physics
University of California, Los Angeles, 2019
Professor Wes Campbell, Chair

The dissertation of Gary Chen is approved.

Eric Hudson

Paul Hamilton

James Larkin

Wes Campbell, Committee Chair

University of California, Los Angeles

2019

Noodle and Nugget

Contents

List of Figures

Preface

Curriculum Vitae

2009 – 2013	B.S. in Physics, University of Maryland (UMD), College Park, Maryland
2013 – Present	Ph.D. student in Physics, University of California, Los Angeles (UCLA).

CHAPTER 1

Introduction

This thesis chronicles the experimental work done to realize an apparatus for cold ion-molecule chemistry of species of astrochemical interest.

1.1 Thesis Outline

CHAPTER 2

The Cryogenic Buffer Gas Beam (CBGB)

To reach reaction temperatures in the regime of 10K from a beam of molecules with trapped ions, a cryogenic buffer gas beam (CBGB) of neon with entrained water is employed. Numerous methods of creating cold beams of molecules exist, from Zeeman decelerators [31], Stark decelerators, to cryogenic buffer gas beams (CBGB). CBGB's in particular have the benefit of being species agnostic, where the resultant beam properties are not dependent on the target species at hand, rather, the buffer gas species.

By holding a cell filled with a noble gas above its vapor pressure, a volume of gas can be held at cryogenic temperatures. Other species of molecules or atoms may be introduced into the buffer gas cell via ablation, fill line, etc. The target species particles are then sympathetically cooled via collisions with the cold buffer gas. An aperture at one end of the cell allows for the extraction of the buffer gas and entrained target species into a ballistic beam. Holding the buffer gas cell temperature to above 17K for neon, and 4K for helium, in high vacuum allows us to accumulate an appreciable stagnation number density within the cell to produce a beam.

The Reynolds number is typically used to characterize the flow regime of the buffer gas beam. At the aperture of the buffer gas cell, the Reynolds number can be written as:

$$\begin{aligned} Re &\approx \frac{2d_{aperture}}{\lambda} \\ &\approx \frac{8\sqrt{2}\dot{N}\sigma}{d_{aperture}\bar{v}} \end{aligned} \tag{2.1}$$

Where $d_{aperture}$ is the diameter of the aperture and λ is the mean free path of the buffer gas

Add citations for decelerators

Add graphic to show what a buffer gas beam is

particles.[22] When the Reynolds number is low, $Re < 1$, we find that there are on average > 1 collisions at the aperture, meaning the particles escape with little to no interactions with other particles and is called the effusive regime. At high Reynolds numbers, $Re > 100$, in the supersonic regime, there are many collisions and forward velocity boosting as well as internal velocity distribution narrowing occurs. In between, we find the intermediate regime, where we observe the onset of hydrodynamic entrainment of target species with mild forward velocity boosting. In all cases, the gasses inside the cell at thermal equilibrium follow the Maxwell-Boltzmann distribution.

$$f(v) = \left(\frac{m}{2\pi kT}\right)^{3/2} 4\pi v^2 e^{-\frac{mv^2}{2kT}} \tag{2.2}$$

Where the mean velocity is:

$$\bar{v} = \sqrt{\frac{8k_B T}{\pi m}} \tag{2.3}$$

2.1 Design Considerations

The CBGB apparatus design is separated by various stages, from a room temperature 300K outer aluminum vacuum can, a nominally 40K aluminum radiation shield, and an inner 4K copper cryopumping surface. A Cryomech PT415 Pulse Tube Refrigerator (PTR) with a remote head option was inserted into the chamber to provide the cooling surfaces. A large bellows attachment connected the pulse tube cooler head to the chamber itself to isolate the chamber from the mechanical vibrations caused by the pulse tube cooler itself.

The PTR itself has 2 cooling stages, and a room temperature stage that mounts to the top plate of the chamber, which in turn houses all of the external connectors into the volume from gas inlets to electrical connections. A 40K cooling stage has 40W of cooling power, while the lowest 4K stage has only 4W. The low cooling power of the lowest stage means that extra care is needed to minimize the heat transfer to the stage from the higher temperature regions. The aluminum radiation shield blocks the vast majority of 300K black

body radiation, while providing windows to view the cell and beam line. The copper region has the experimental cell, encompassed by a copper enclosure that acts as a cryopumping surface at the appropriate temperatures. Because it is heat sunk into the same cooling stage as the experimental cell, the copper enclosure does not act as a radiation shield.

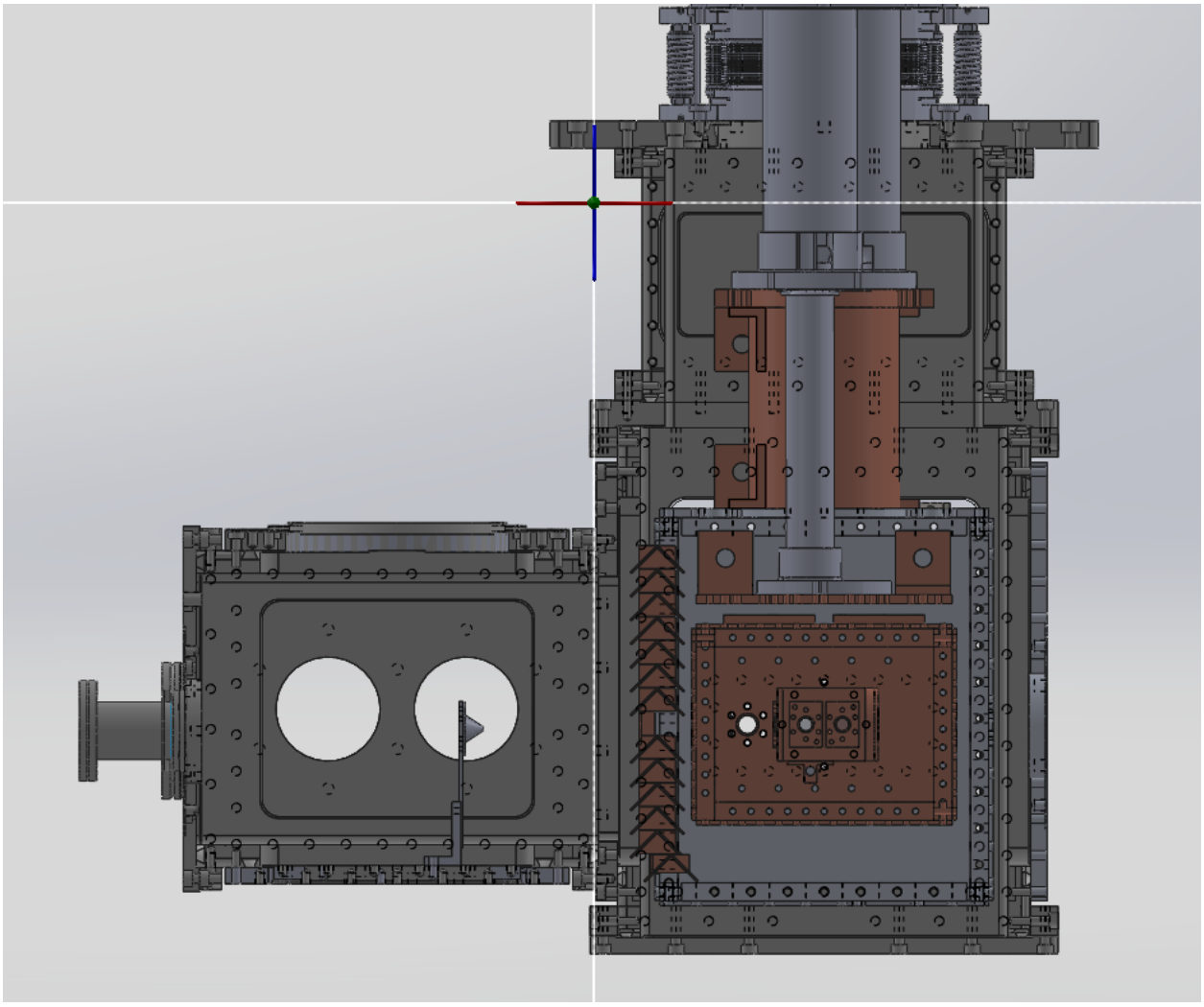

Figure 2.1: Cross sectional view of CBGB in solidworks.

The mounting of the inner components was of particular importance due to the fragility of the PTR as well as the desire to minimize thermal conductivity to the experimental region. All the shield components were mounted to the top mounting plate

solidworks image of system

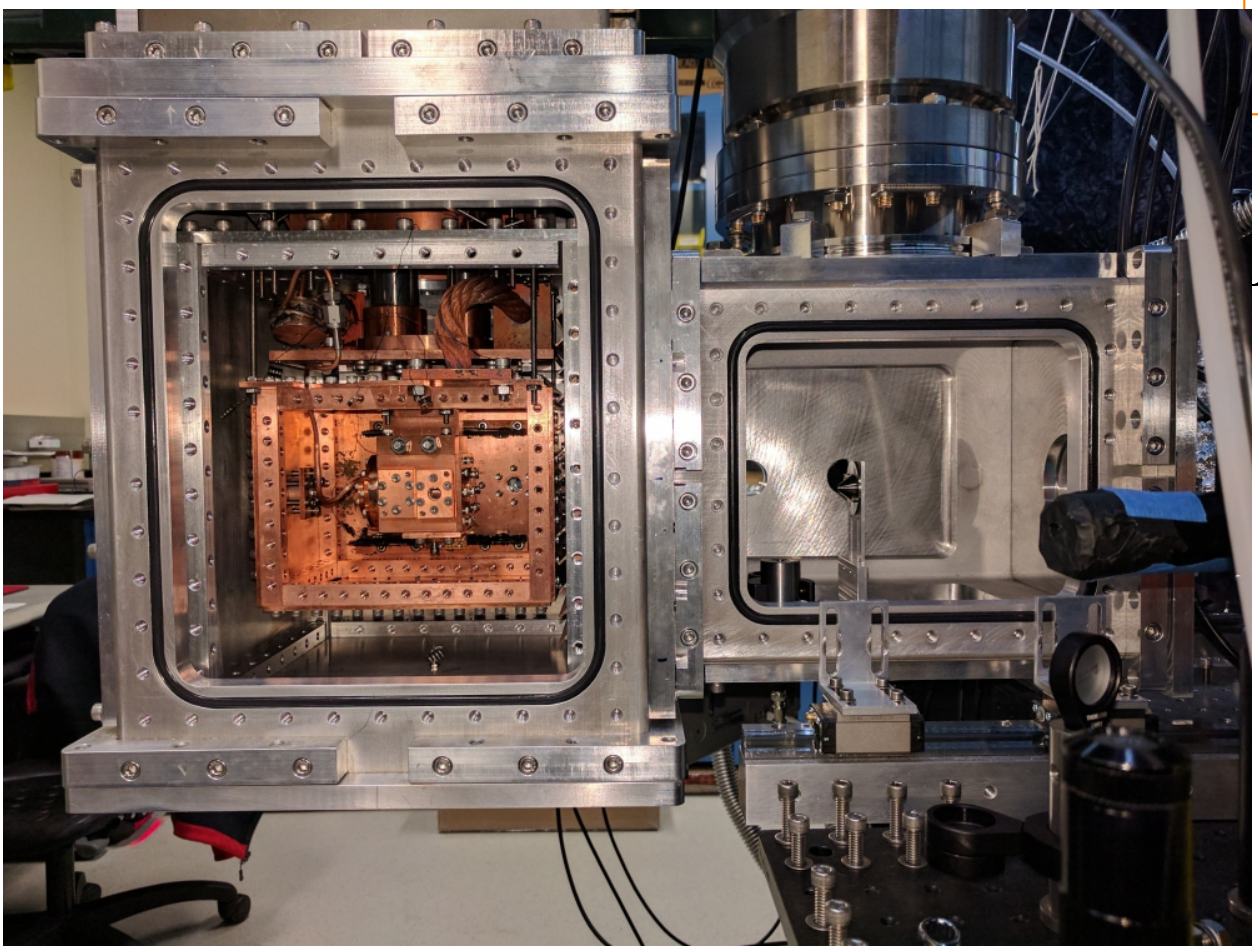

Figure 2.2: Cross sectional view of CBGB with side walls removed from the outer vacuum chamber, 40K aluminum radiation shield, and inner 4K cryopumping shield exposing the inner experimental cell. A skimmer is mounted in the stem region.

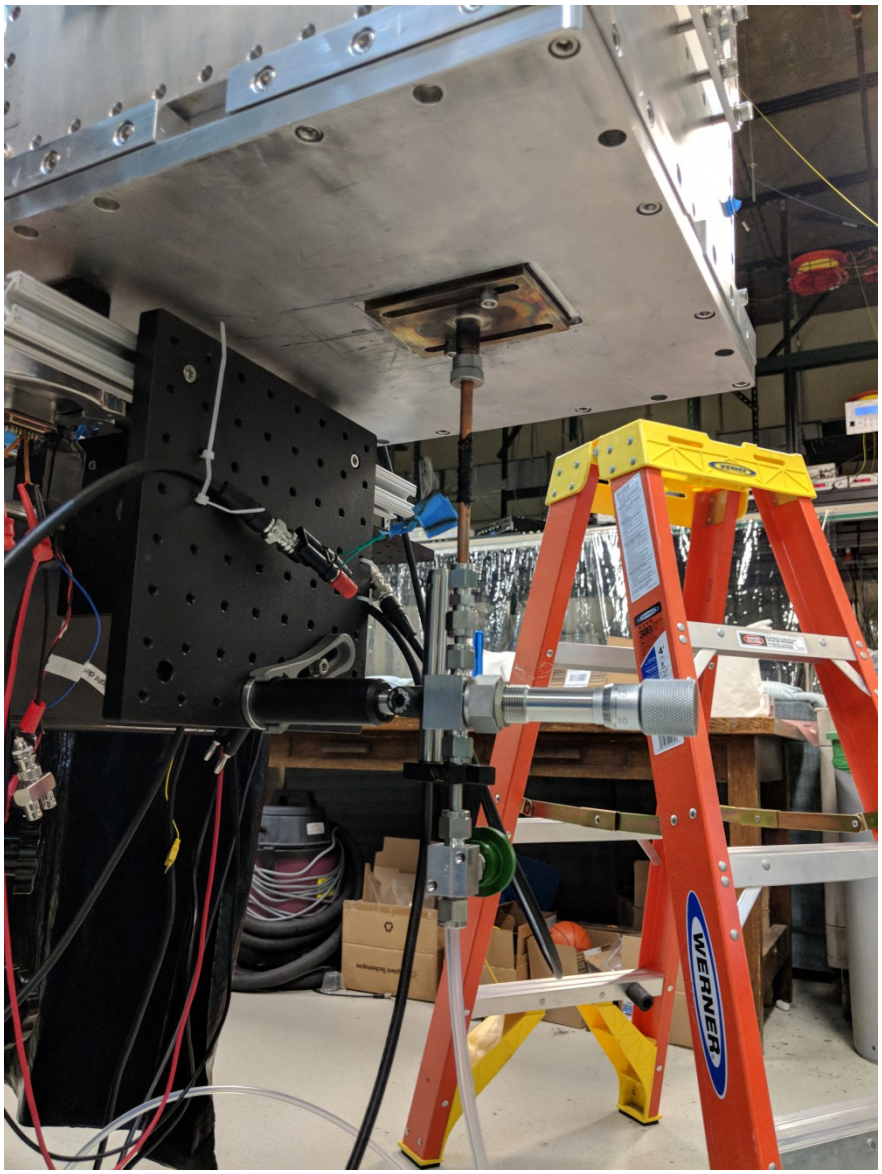

Figure 2.3: The water fill line, sealed by an ultratorr fitting and heated by nichrome wire. A shut off valve and vernier valve are used to regulate the flow of water into the buffer gas cell.

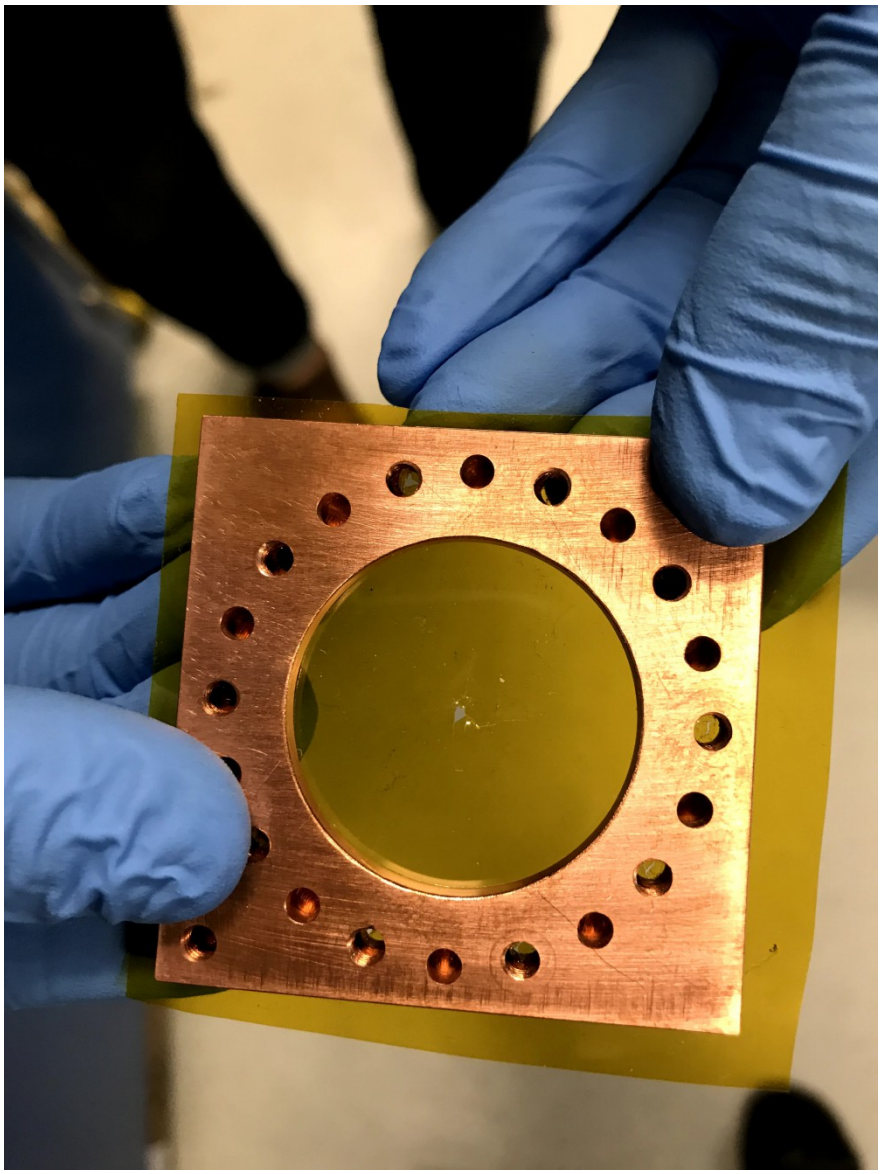

Figure 2.4: A kapton film serves as the back wall of the buffer gas cell with a hole for the insertion of the water fill line. The kapton surface resists ice formation and allows for continuous operation with water for over 10 hours.

2.2 Beam Density and Extraction

The stagnation density inside the buffer gas cell is a function of the physical dimensions of the cell and the number flow rate into the cell. High stagnation densities allows for high

densities of reactants at the ion trap center, but can push the beam into an unwanted flow regime where the beam properties are not what one wants. Experimentally, it's preferable to use volumetric flow rates when operating the apparatus, but for calculations, that needs to translate to number flow rate using the ideal gas law:

$$\dot{N} = \frac{Pf}{k_B T}$$

where P is pressure and f is the volumetric flow rate, this translates to about 4×10^{17}particles/s^{-1} for 1SCCM of gas flow. By solving for the number density in the flow out of an aperture with molecular flow, we find that the stagnation density within the cell can be shown as:

$$n_b = \frac{4\dot{N}}{A_{aperture}\bar{v}}$$

In general, buffer gas beams operate with stagnation densities around $10^{15} - 10^{17}$cm^{-3}. Outside of the cell, we can describe the density of the beam as a function of distance. [33]

$$n(z) = \frac{n_0}{2}\left(1 - \frac{z}{\sqrt{z^2 + a^2}}\right) \tag{2.4}$$

Where z is the distance from the aperture into the vacuum side, n_0 is the initial number density, a is the radius of the aperture. In the far-field, this goes to:

$$n(z) = \frac{n_0 a^2}{4z^2}$$

But there is something that we must consider, that is that we aren't seeing the full aperture while we are at all locations, we are actually seeing an appended area due to the inclusion of apertures and skimmers in the way. So in the calculation for $n(z)$, only n_0 has a dependence on the aperture size of the cell, $n(z)$ itself will have a set value defined by the smallest aperture in the beam path. For us, although our cell aperture is $\approx$ 9mm in diameter, we have multiple apertures and skimmers in the way, of which, a skimmer from with a diameter of 2mm is used.

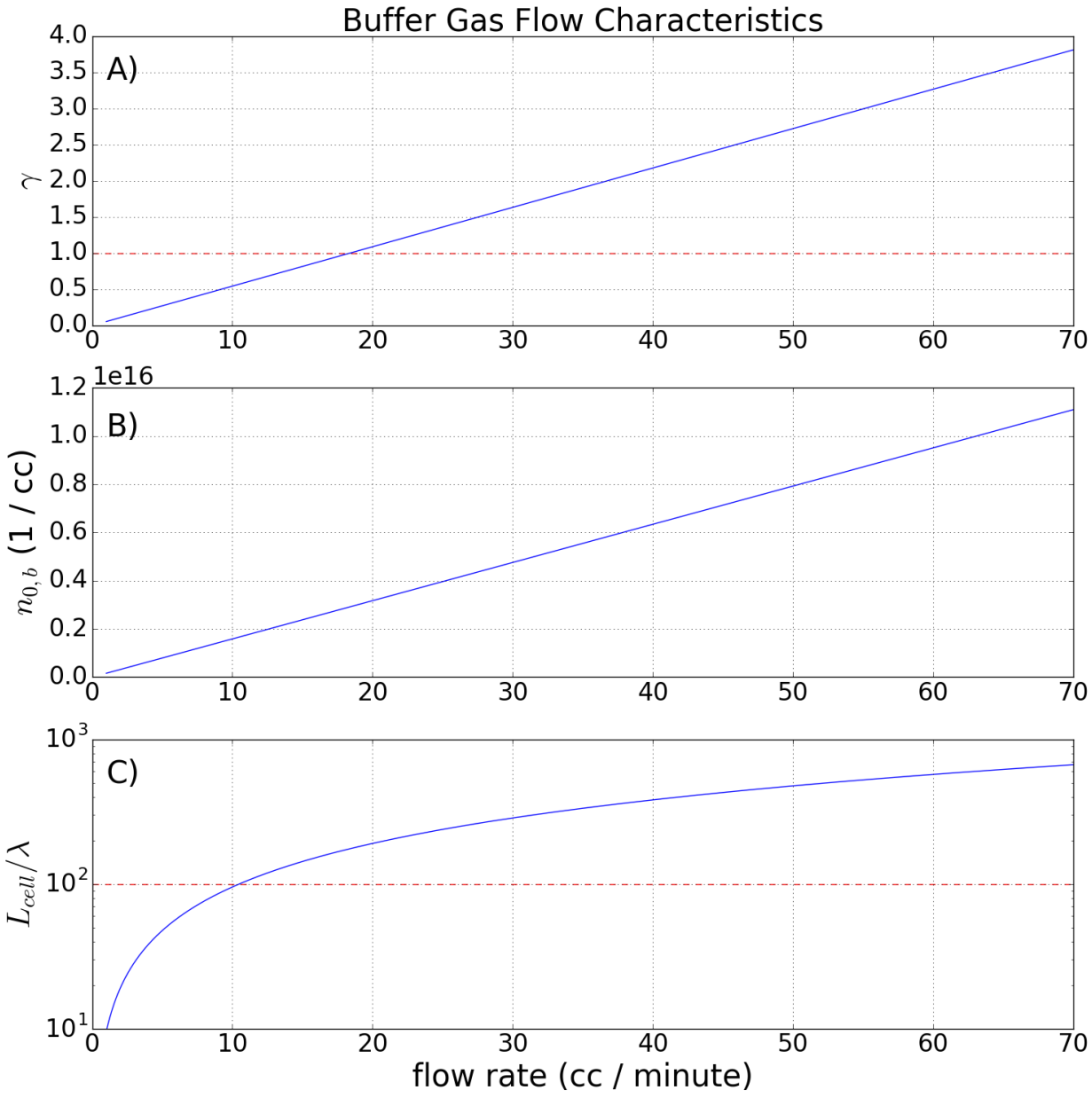

Figure 2.5: A) γ extraction ratio, dotted red line indicates $\gamma = 1$ where hydrodynamic entrainment begins. B) Theoretical number density of buffer gas species within buffer gas cell. The density of target species introduced should stay under 1% of the buffer gas density. C) Number of collisions a target species particle would expect before extraction out of the cell, the dotted red line indicates 100 collisions before extraction when rotational degrees of freedom are characteristically thermalized.

Sympathetic cooling occurs through collisions between the hot target species being introduced and the cryogenic buffer gas particles. The thermalization of the target species with the buffer gas particles is derived via momentum conservation of hard sphere collisions, where ≈ 10 and ≈ 100 collisions are needed to relax translational and rotational states to within a factor of 2 of the buffer gas temperature. Vibrational degrees of freedom may take upwards of 10^4 collisions to fully thermalize is the elastic collision energy is much lower than the internal vibrational level. By finding the mean free path, we can consider the characteristic length the particles travel to be thermalized with the buffer gas, this is then compared to the characteristic length of the cell to determine the effectiveness of the cooling.

$$\lambda = \frac{A_{aperture}\bar{v}}{4f\sigma\sqrt{m_s/m_b}}$$

If a species is introduced into the buffer gas cell that has a lower vapor pressure than that is allowed at the current temperature, it will be lost when it comes in contact with the cell walls. The rate of this loss can be described as the characteristic time of diffusion of a particle in the buffer gas to the physical dimensions of the cell set the diffusion time constant:

$$\tau_{diff} = \frac{16}{9\pi}\frac{A_{cell}n_{0,b}\sigma}{\bar{v}} \tag{2.5}$$

where σ represents the collisional cross section for the buffer gas with the target species. On the other hand, we have the characteristic pump out time given by the conductance of a cell aperture:

$$\tau_{pump} = \frac{4V_{cell}}{\bar{v}A_{aperture}} \tag{2.6}$$

By combining equations eqs. (2.5) and (2.6), we can get a dimensionless ratio, γ that characterizes the extraction fraction out of the cell.

$$\gamma = \frac{\tau_{diff}}{\tau_{pump}} = \frac{\sigma f}{L_{cell}\bar{v}} \tag{2.7}$$

Notice that the γ factor does not depend on aperture size, this is generally true, but increasing the aperture size will lower your number density within the cell, which then influences the characteristic length scale of thermalization. Larger apertures thus run the risk of not allowing your particles to fully thermalize in rotational/vibrational states. But decreasing the aperture size can make alignment as well as controlling the number density more difficult, as finer control over the flow rate is necessary for equivalent flow regimes.

We have utilized a residual gas analyzer (RGA) to determine the density of the beam in the ballistic regime upstream from the ion trap. Inserting the RGA into the beam path allows us to estimate the density of water in the beam as a function of the nominal buffer gas flow rate, as shown in figure 2.6. Using that fit, we find good agreement with the theoretical calculations showing our flow to be near the supersonic regime, while staying in the hydrodynamic regime with a linear extraction efficiency dependence with the flow rate expressed in 2.7.

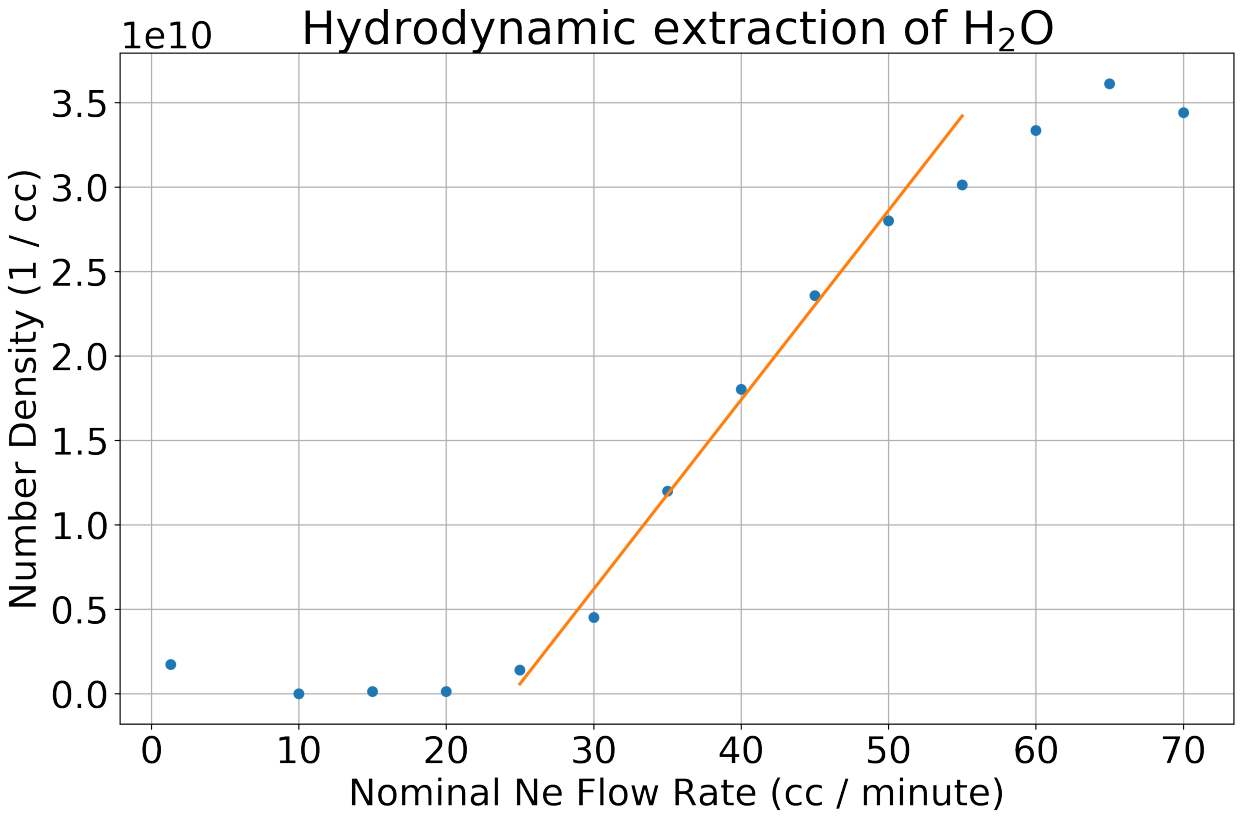

Figure 2.6: $1.12 \times 10^{9}x + -2.75 \times 10^{1}0$

We know have previously calculated the possible number densities of the buffer gas with varying aperture sizes and flow rates. But now we can utilize those equations with the data on the target species to plot out the range of densities that we may see at the trap center as a function of the various apertures that we may utilize.

Knowing from our previous calculations:

$$\bar{v} = \sqrt{\frac{8k_BT}{m\pi}}$$
$$n_{0,b} = \frac{4f}{A_{aperture}\bar{v}}$$
$$n(z) = \frac{n_o}{2}\left(1 - \frac{z}{\sqrt{z^2 + a^2}}\right)$$

We can put it all together to get:

$$n(z) = \alpha \frac{f}{A_{aperture}\bar{v}} \left(1 - \frac{z}{\sqrt{z^2 + a^2}}\right)$$

But what we really care about is the region in which the number density is linearly dependent to the buffer gas flow rate, not over all possible ranges; we've seen that the target species only behaves linearly once it has been entrained in the buffer gas. This means that we should be equating the density function with the linear fit performed on the data for the parameters the data was taken at, $n(z) = mf + b$.

$$\alpha = \frac{m}{\beta} + \frac{b}{\beta f}$$

Where we let $\beta = \frac{1}{A_{aperture,0}\bar{v_0}} \left(1 - \frac{z_0}{\sqrt{z_0^2 + a_0^2}}\right)$. Thus, we may get a final form that incorporates the linear slope's dependence on the other variables of the system as well as the overall experimentally derived scaling factor from the data.

$$n(z) = \frac{mf + b}{A_{aperture}\bar{v}\beta} \left(1 - \frac{z}{\sqrt{z^2 + a^2}}\right)$$

There is a mass dependence in the thermal velocity equation, which leads us to conclude that the choice of the species is a statement of the effecacy of the beam itself. If we choose to calculate the thermal velocity of the target species found in the beam due to the theoretical thermal velocity of the buffer gas, that indicates that the beam properties are still dominated by the buffer gas species. This may not be the case, as we see in our data, we have a ratio of about 10:1, this is pushing the boundaries of the assumption that the buffer gas far outnumbers the target species. At these ratios, we may start to see the effects of the target species on the beam properties.

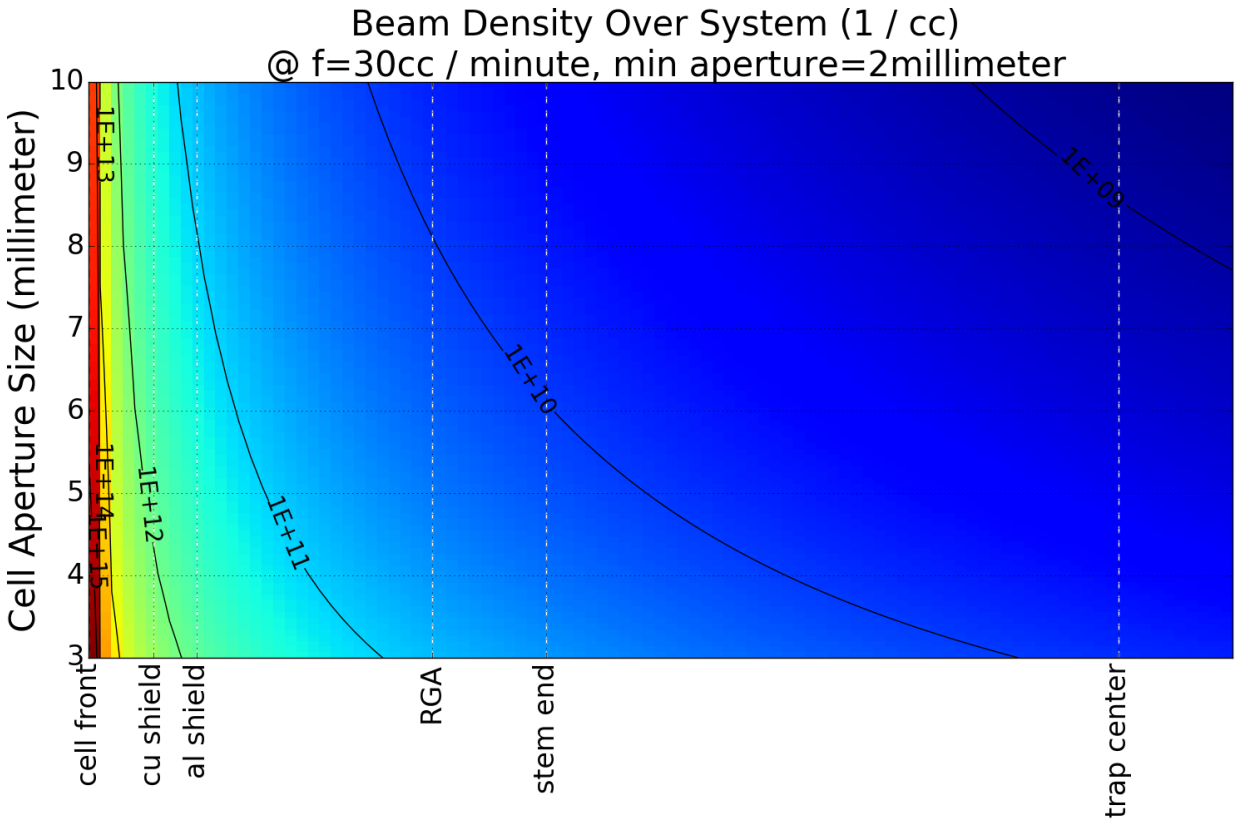

Figure 2.7: Projected buffer gas beam densities with a Ne flow rate of 30SCCM with various distances of interest within the chamber. Optimal densities of entrained gasses hover around 0.1% of the buffer gas value shown here.

Extrapolating the fit and estimated density from figure 2.6, we can estimate the density of the water at various locations along the beam line as shown in figure 2.7. We find that we should be able to produce an appreciable number density of water down at the trap center.

From the RGA, we were able to open and close a shutter in the beam path and see an extinction of the water signal, but a more accurate representation would be from the ions in the trap themselves. We know that the trapped Be^+ ions will reaction with H_2O to predominately produce $BeOH$, which we see as a drop in the fluorescence. Figure 2.2 shows fits of the fluorescence decay as a beam from the CBGB is suddenly blocked by our shutter in the beam line. Comparing the fitted reaction rates, we find that they agree with

the background rates found as shown in figure 2.2. This indicates to us that we indeed have a beam of cryogenic water coming from the CBGB, as seen by the sudden extinction of the $Be^+ + H_2O$ reaction.

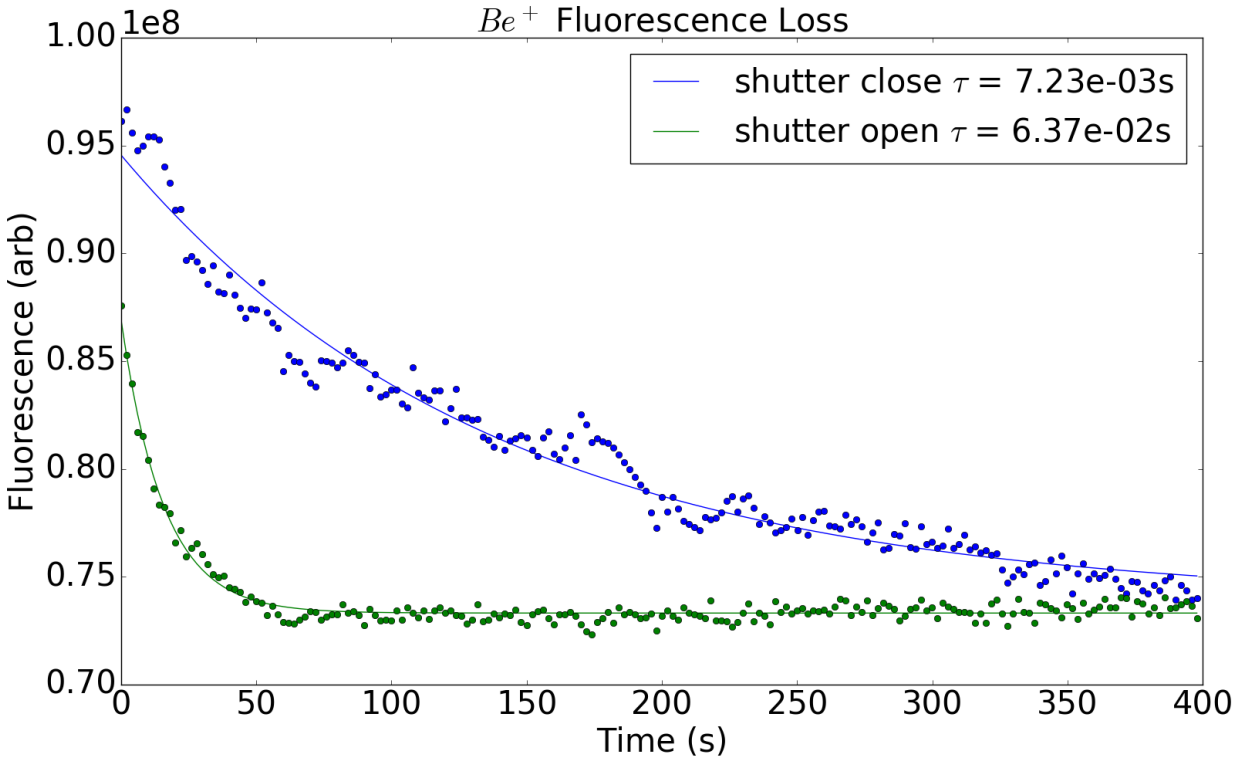

Figure 2.8:

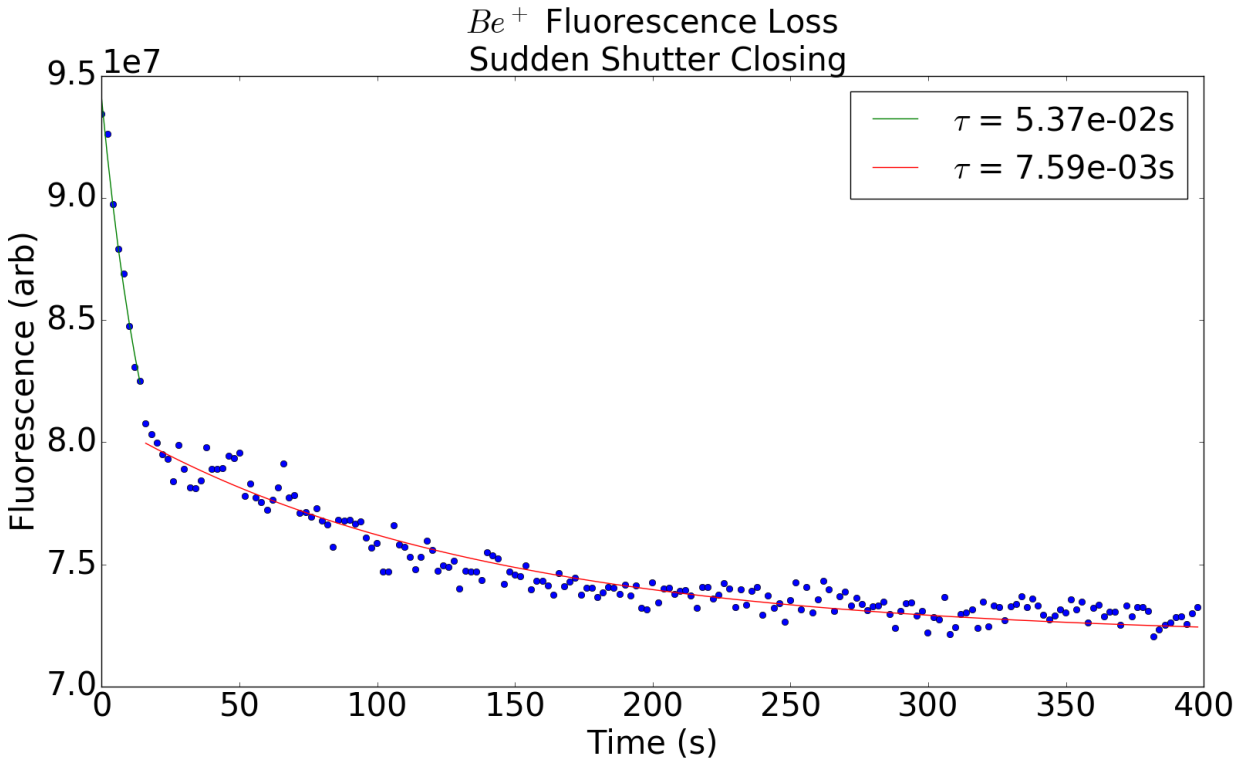

Figure 2.9:

2.3 Beam Velocity

We may rewrite the equation 2.2 as a function of the mean velocity $\bar{v}$ into a simpler form .

$$f(v) = \frac{32}{\pi^2}\frac{v^2}{\bar{v}^3}e^{-4v^2/\pi\bar{v}^2} \tag{2.8}$$

To get the velocity distribution in the beam, we can calculate the distribution of particles incident on an aperture in the cell.

$$\begin{aligned} f_{beam}(v) &= \frac{v}{\bar{v}}f(v) \\ &= \frac{32}{\pi^2}\frac{v^3}{\bar{v}^4}e^{-4v^2/\pi\bar{v}^2} \end{aligned}$$

For low Reynold's numbers (Re<1) the flow at the aperture is purely molecular, which means that there are few to no collisions. This allows us to continue to use the Maxwell-Boltzmann distribution to describe the forward velocity [23].

$$\bar{v}_{\parallel} = \int_0^{\infty} v f(v) dv \approx 1.2\bar{v} \tag{2.9}$$

The spread of the forward velocity of an effusive beam is the full width half max (FWHM) of the Maxwell-Boltzmann distribution: $\Delta\bar{v} \approx 1.5\bar{v}$. As the Reynolds number increases, one can reach the supersonic regime (Re>100) where the forward velocity reaches $1.4\bar{v}$ and the distribution drastically narrows.[23, 33]

But as the flow regime nears the supersonic regime, forward collisions around the aperture cause boosting of the average velocity as well as a decrease in the velocity spread. Changing the flow regime may also change the ratio of species in the beam as well.

A helium buffer gas held at 4K will have a slower forward velocity than that of a neon gas held at 17K. Despite this, it is preferable to use neon as a buffer gas due to its ideal cryopumping properties. Helium requires large amounts of activated charcoal, also held at low temperatures, to effectively cryopump. These volumes of charcoal can then become saturated and require purging, limiting one's operating time (few hours). Neon on the other hand, only requires a metal surface lower than 17K to create neon ice. The neon ice surface will then act as a cryopump for more neon gas as well, allowing for many hours of continuous operation with no appreciable build up of background gas. Our experiment uses neon as a buffer gas for its technical simplicity, the lower achievable temperature with the helium does not yield dramatic gains in the final reaction temperature.

To better understand the reaction temperatures we will be able to reach, we need a characterization of the beam's velocity, more specifically, the velocity of the target species entrained within the buffer gas. By ablating ytterbium into the neon buffer gas, we find that the ytterbium is entrained within the neon and sympathetically cooled to the cell's temperature. As long as the target species number density is a trace amount in comparison to the bulk buffer gas number density (1:1000), the flow characteristics are dominated by

the buffer gas species [22]. The forward velocity of the beam is not only parameterized by the temperature of the buffer gas species, it is also dependent on the flow regime. As we increase the flow of neon into the cell, figure 2.6 shows a linear increase in the H_2O signal from a downstream RGA. This coincides with the beam operating within the intermediate flow regime, where there are few collisions at the cell aperture, resulting in a slight forward boosting and increased extraction efficiency of the target species. At higher flow regimes, entering the supersonic regime, we would see a "freeze out" where the forward velocity reaches $1.4\bar{v}$ and we would not see appreciable gains in species extraction [22]. We chose to operate at a nominal neon flow rate of 30 sccm based upon the reaction rate of the ions downstream.

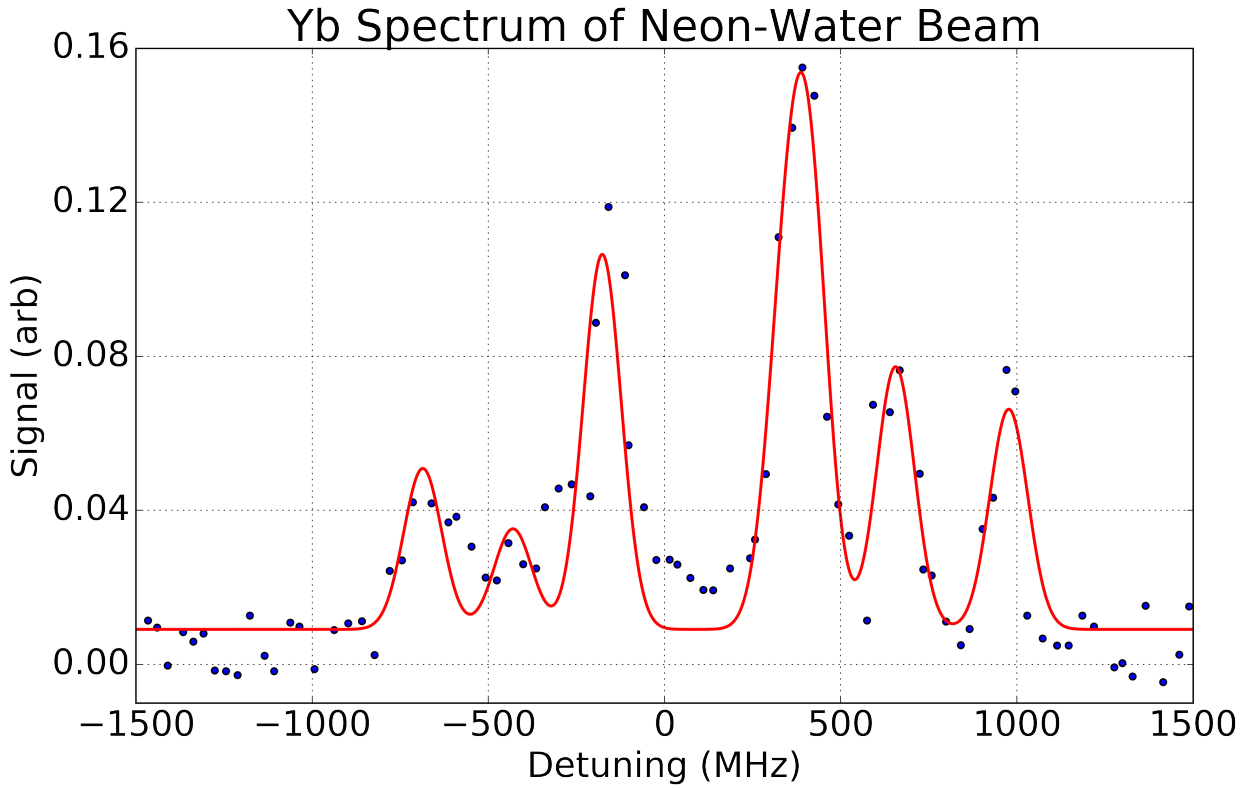

Figure 2.10:

CHAPTER 3

Linear Quadrupole Trap (LQT)

3.1 Ion Trapping

3.2 Dual Species Loading

3.3 Time of Flight Mass Spectrometer (TOF-MS)

References

[1] N. G. Adams and D. Smith. The selected ion flow tube (SIFT); A technique for studying ion-neutral reactions. *International Journal of Mass Spectrometry and Ion Physics*, 21(3-4):349–359, 1976.

[2] Marcelino Agúndez and Valentine Wakelam. Chemistry of Dark Clouds: Databases, Networks, and Models. *Chemical Reviews*, 113(12):8710–8737, 2013.

[3] PB Armentrout. Reactions and Therochemistry of Small Transition Metal Cluster Ions. *Annual Review of Physical Chemistry*, 52(1):423–461, 2002.

[4] J J Bollinger, J S Wells, D J Wineland, and Wayne M Itano. Hyperfine structure of the $2p^2P_{1/2}$ state in $^9Be^+$. *Physical Review A*, 31(4):2711–2714, 1985.

[5] Michael J. Bronikowski, William R. Simpson, Bertrand Girard, and Richard N. Zare. Bond-specific chemistry: OD:OH product ratios for the reactions H+HOD(100) and H+HOD(001). *Journal of Chemical Physics*, 95(11):8647–8648, 1991.

[6] Eduardo Carrascosa, Jennifer Meyer, and Roland Wester. Imaging the dynamics of ion-molecule reactions. *Chemical Society Reviews*, 46(24):7498–7516, 2017.

[7] Kuang Chen, Scott T. Sullivan, and Eric R. Hudson. Neutral gas sympathetic cooling of an ion in a Paul trap. *Physical Review Letters*, 112(14):1–5, 2014.

[8] Kuang Chen, Scott T. Sullivan, Wade G. Rellergert, and Eric R. Hudson. Measurement of the coulomb logarithm in a radio-frequency Paul trap. *Physical Review Letters*, 110(17):1–5, 2013.

[9] D. C Clary. Fast Chemical Reactions: Theory Challenges Experiment. *Annual Review of Physical Chemistry*, 41(1):61–90, 1990.

[10] F. Fleming Crim. Bond-selected chemistry: Vibrational state control of photodissociation and bimolecular reaction. *Journal of Physical Chemistry*, 100(31):12725–12734, 1996.

[11] N. F. Dalleska, Kevin C. Crellin, and P. B. Armentrout. Reactions of alkaline earth ions with hydrogen, deuterium, and hydrogen deuteride. *The Journal of Physical Chemistry*, 97(13):3123–3128, 2005.

[12] C. E. Dateo and D. C. Clary. Rate constant calculations on the C^+ + HCl reaction. *The Journal of Chemical Physics*, 1989.

[13] Colin G. Freeman, John S. Knight, Jonathan G. Love, and Murray J. McEwan. The reactivity of HOC^+ and the proton affinity of CO at O. *International Journal of Mass Spectrometry and Ion Processes*, 80(C):255–271, 1987.

[14] Colin G. Freeman and Murray J. McEwan. A selected-ion flow tube study of the $C^+ + H_2O$ reaction. *International Journal of Mass Spectrometry and Ion Processes*, 75(1):127–131, 1987.

[15] Bina Fu and Dong H. Zhang. A full-dimensional quantum dynamics study of the mode specificity in the H + HOD abstraction reaction. *Journal of Chemical Physics*, 142(6), 2015.

[16] George Gioumousis and D. P. Stevenson. Reactions of gaseous molecule ions with gaseous molecules. V. theory. *The Journal of Chemical Physics*, 29(2):294–299, 1958.

[17] Anders K. Hansen, Magnus A. Sørensen, Peter F. Staanum, and Michael Drewsen. Single-ion recycling reactions. *Angewandte Chemie - International Edition*, 51(32):7960–7962, 2012.

[18] William L. Hase, Jochen Mikosch, Roland Wester, Jiaxu Zhang, Rico Otto, and Jing Xie. Identification of Atomic-Level Mechanisms for Gas-Phase $X^- + CH_3$ Y S_N2 Reactions by Combined Experiments and Simulations. *Accounts of Chemical Research*, 47(10):2960–2969, 2014.

[19] J L Highberger, C Savage, J H Bieging, and L M Ziurys. HEAVY-METAL CHEMISTRY IN PROTO-PLANETARY NEBULAE: DETECTION OF MgNC, NaCN, AND AlF TOWARD CRL 2688. *the Astrophysical Journal*, 562:790–798, 2001.

[20] Eric R. Hudson. Sympathetic cooling of molecular ions with ultracold atoms. *EPJ Techniques and Instrumentation*, 3(1):8, 2016.

[21] W. T. Huntress and R. F. Pinizzotto. Product distributions and rate constants for ion-molecule reactions in water, hydrogen sulfide, ammonia, and methane. *The Journal of Chemical Physics*, 59(9):4742–4756, 2004.

[22] Nicholas R Hutzler, Hsin-I Lu, and John M Doyle. The buffer gas beam: an intense, cold, and slow source for atoms and molecules. *Chemical reviews*, 112(9):4803–27, sep 2012.

[23] NR Nicholas R Hutzler, MF Maxwell F Parsons, Yulia V Gurevich, Paul W Hess, Elizabeth Petrik, Ben Spaun, Amar C Vutha, David Demille, Gerald Gabrielse, and John M Doyle. A cryogenic beam of refractory, chemically reactive molecules with expansion cooling. ... *Chemistry Chemical ...*, 13(42):1–16, 2011.

[24] Vladimir A Krasnopolsky. Chemical composition of Titan's atmosphere and ionosphere: Observations and the photochemical model. *Icarus*, 236:83–91, 2014.

[25] D. J. Larson, J. C. Bergquist, J. J. Bollinger, Wayne M. Itano, and D. J. Wineland. Sympathetic cooling of trapped ions: A laser-cooled two-species nonneutral ion plasma. *Physical Review Letters*, 57(1):70–73, 1986.

[26] Adan Li, Jianzheng Song, Yang Sun, and Tifeng Jiao. The application of resonance-enhanced multiphoton ionization technique in gas chromatography mass spectrometry. *Journal of Spectroscopy*, 2014, 2014.

[27] Jun Li, Bin Jiang, and Hua Guo. Spin-orbit corrected full-dimensional potential energy surfaces for the two lowest-lying electronic states of FH_2O and dynamics for the F + $H_2O \rightarrow$ HF + OH reaction. *Journal of Chemical Physics*, 138(7), 2013.

[28] Jun Li, Bin Jiang, Hongwei Song, Jianyi Ma, Bin Zhao, Richard Dawes, and Hua Guo. From ab initio potential energy surfaces to state-resolved reactivities: X + $H_2O \leftrightarrow$ HX + OH [X = F, Cl, and O(^{3}P)] reactions. *Journal of Physical Chemistry A*, 119(20):4667–4687, 2015.

[29] U. Lourderaj, M. Weidemuller, W. L. Hase, J. Mikosch, R. Otto, R. Wester, C. Eichhorn, J. X. Zhang, and S. Trippel. Imaging Nucleophilic Substitution Dynamics. *Science*, 319(5860):183–186, 2008.

[30] Ricardo B. Metz, John D. Thoemke, Joann M. Pfeiffer, and F. Fleming Crim. Selectively breaking either bond in the bimolecular reaction of HOD with hydrogen atoms. *Journal of Chemical Physics*, 99(3):1744–1751, 1993.

[31] Edvardas Narevicius, Adam Libson, Christian G. Parthey, Isaac Chavez, Julia Narevicius, Uzi Even, and Mark G. Raizen. Stopping supersonic oxygen with a series of pulsed electromagnetic coils: A molecular coilgun. *Physical Review A - Atomic, Molecular, and Optical Physics*, 77(5):1–4, 2008.

[32] M. Oppenheimer and A. Dalgarno. The Fractional Ionization in Dense Interstellar Clouds. *The Astrophysical Journal*, 192(12):29, 2002.

[33] Hans Pauly. *Atom, Molecule, and Cluster Beams I: Basic Theory, Production and Detection of Thermal Energy Beams*, volume 28. Springer, 2000.

[34] Prateek Puri, Michael Mills, Christian Schneider, Ionel Simbotin, John A. Montgomery, Robin Côté, Arthur G. Suits, and Eric R. Hudson. Synthesis of mixed hypermetallic oxide $BaOCa^+$ from laser-cooled reagents in an atom-ion hybrid trap. *Science*, 357(6358):1370–1375, 2017.

[35] Amelia W. Ray, Jianyi Ma, Rico Otto, Jun Li, Hua Guo, and Robert E. Continetti. Effects of vibrational excitation on the F + H2O $\rightarrow$ HF + OH reaction: Dissociative photodetachment of overtone-excited [F-H-OH]$^-$. *Chemical Science*, 8(11):7821–7833, 2017.

[36] B. Roth, P. Blythe, H. Wenz, H. Daerr, and S. Schiller. Ion-neutral chemical reactions between ultracold localized ions and neutral molecules with single-particle resolution. *Physical Review A - Atomic, Molecular, and Optical Physics*, 73(4):1–9, 2006.

[37] Christian Schneider, Steven J. Schowalter, Kuang Chen, Scott T. Sullivan, and Eric R. Hudson. Laser-Cooling-Assisted Mass Spectrometry. *Physical Review Applied*, 2(3):1–7, 2014.

[38] Steven J. Schowalter, Kuang Chen, Wade G. Rellergert, Scott T. Sullivan, and Eric R. Hudson. An integrated ion trap and time-of-flight mass spectrometer for chemical and photo- reaction dynamics studies. *Review of Scientific Instruments*, 83(4), 2012.

[39] Steven J. Schowalter, Alexander J. Dunning, Kuang Chen, Prateek Puri, Christian Schneider, and Eric R. Hudson. Blue-sky bifurcation of ion energies and the limits of neutral-gas sympathetic cooling of trapped ions. *Nature Communications*, 7:1–8, 2016.

[40] Ian R Sims. Gas-Phase Reactions and Energy Transfer at Very Low Temperatures. *Annual Review of Physical Chemistry*, 46(1):109–137, 2002.

[41] Amitabha Sinha, Mark C. Hsiao, and F. Fleming Crim. Bond-selected bimolecular chemistry: H+HOD($4\nu_{OH}$)→OD+H_2. *The Journal of Chemical Physics*, 92(10):6333–6335, 1990.

[42] Dimitris Skouteris, David E. Manolopoulos, Wensheng Bian, Hans Joachim Werner, Lih Huey Lai, and Kopin Liu. Van der Waals interactions in the Cl + HD reaction. *Science*, 286(5445):1713–1716, 1999.

[43] I. W M Smith and Bertrand R. Rowe. Reaction kinetics at very low temperatures: Laboratory studies and interstellar chemistry. *Accounts of Chemical Research*, 33(5):261–268, 2000.

[44] Theodore P. Snow and Veronica M. Bierbaum. Ion Chemistry in the Interstellar Medium. *Annual Review of Analytical Chemistry*, 1(1):229–259, 2008.

[45] Hongwei Song and Hua Guo. Vibrational and Rotational Mode Specificity in the Cl + H_2O → HCl + OH Reaction: A Quantum Dynamical Study. *Journal of Physical Chemistry A*, 119(24):6188–6194, 2015.

[46] Hongwei Song, Soo Ying Lee, Yunpeng Lu, and Hua Guo. Full-Dimensional Quantum Dynamical Studies of the Cl + HOD→HCl/DCl + OD/OH Reaction: Bond Selectivity and Isotopic Branching Ratio. *Journal of Physical Chemistry A*, 119(50):12224–12230, 2015.

[47] Timothy Su and Michael T. Bowers. Ion-polar molecule collisions: the effect of ion size on ion-polar molecule rate constants; the parameterization of the average-dipole-orientation theory. *International Journal of Mass Spectrometry and Ion Physics*, 12(4):347–356, 1973.

[48] Timothy Su and Michael T. Bowers. Theory of ion-polar molecule collisions. Comparison with experimental charge transfer reactions of rare gas ions to geometric isomers of difluorobenzene and dichloroethylene. *The Journal of Chemical Physics*, 58(7):3027–3037, 1973.

[49] Timothy Su and Michael T. Bowers. Ion-polar molecular collisions: the average quadrupole orientation theory. *International Journal of Mass Spectrometry and Ion Physics*, 17(3):309–319, 1975.

[50] Michał Tomza, Krzysztof Jachymski, Rene Gerritsma, Antonio Negretti, Tommaso Calarco, Zbigniew Idziaszek, and Paul S. Julienne. Cold hybrid ion-atom systems. pages 1–61, 2017.

[51] J. Troe. Statistical adiabatic channel model of ion-neutral dipole capture rate constants. *Chemical Physics Letters*, 122(5):425–430, 1985.

[52] Ewine F. van Dishoeck, Eric Herbst, and David A. Neufeld. Interstellar Water Chemistry: From Laboratory to Observations. *Chemical Reviews*, 113(12):9043–9085, 2013.

[53] Stefan Willitsch. Coulomb-crystallised molecular ions in traps: Methods, applications, prospects. *International Reviews in Physical Chemistry*, 31(2):175–199, 2012.

[54] D. J. Wineland and Wayne M. Itano. Laser cooling of atoms. *Physical Review A*, 20(4):1521–1540, 1979.

[55] Paul Wolfgang. Electromagnetic Traps For charged And Neutral Particles, 1990.

[56] Chunlei Xiao, Xin Xu, Shu Liu, Tao Wang, Wenrui Dong, Tiangang Yang, Zhigang Sun, Dongxu Dai, Xin Xu, Dong H Zhang, and Xueming Yang. Experimental and theoretical differential cross sections for a four-atom reaction: HD + OH $\rightarrow$ H_2O + D. *Science*, 333(6041):440–442, 2011.

[57] Richard N. Zare. Laser Control of Chemical Reactions. *Science*, 279(5358):1875–1879, 1998.

[58] Dong H Zhang and John C Light. Full-dimensional quantum study. 93(5):691–697, 1997.

[59] Dongdong Zhang and Stefan Willitsch. Cold ion chemistry. 2017.

[60] Rui Zheng, Yongfa Zhu, and Hongwei Song. Mode specific dynamics in bond selective reaction O′(^{3}P) + HOD$\rightarrow$ O′H + OD/O′D + OH. *Journal of Chemical Physics*, 149(5), 2018.